Forces between zinc sulphide surfaces; Amplification of the hydrophobic attraction by surface charge

E-Jen Teh[1], Naoyuki Ishida[2], William M. Skinner[3], Drew Parsons[4] and Vincent S. J. Craig[1]

[1]Department of Applied Mathematics, Research School of Physics, The Australian National University, Mills Rd Acton, Canberra, 2601, Australia

[2] Graduate School of Natural Science and Technology, Okayama University, Okayama, Japan

[3]Future Industries Institute, Mawson Lakes Campus, University of South Australia, Mawson Lakes SA 5095, Australia

[4]School of Engineering & IT, Murdoch University, 60 South St, Murdoch, WA, 6150

Corresponding author: vince.craig@anu.edu.au

Abstract

Smooth Zinc Sulphide (ZnS) surfaces were prepared by magnetron sputtering and the interaction forces measured between them as a function of pH. At the isoelectric point (iep) of pH 7.1 the attractive force was well described by the van der Waals interaction calculated using Lifshitz theory for a layered system. Away from the iep, the forces were fitted using DLVO theory extended to account for surface roughness. At pH 9.8 the surfaces acquire a negative charge and an electrostatic repulsion is evident. Below the iep the surfaces acquire a positive charge leading to electrostatic repulsion. The forces in the range $3.8 < pH < 4.8$ show an additional attraction on approach and much greater adhesion than at other pH values. This is attributed to the hydrophobic attraction being amplified by a small degree of charge on the surface as has previously been reported for adhesion measurements. The range of the measured forces is attributed to the long-range orientational order of water (> 5 nm).

Introduction

Thirty-five years have passed since the first report of the long-range hydrophobic attractive force[1] without resolution of the range of the interaction or the mechanism behind the attraction[2]. In this time the reported forces measured between hydrophobic surfaces in aqueous solutions have varied widely in magnitude, range and in their sensitivity to electrolytes[2-12]. Measurements of the interaction between macroscopic hydrophobic surfaces are complicated by two factors. Firstly, hydrophobic surfaces in water show a propensity for trapping very small bubbles of air that have become known as surface nanobubbles[13-16] and it is difficult to produce surfaces that are sufficiently smooth that do not introduce artifacts or complicate the interpretation of the data[2].

What is apparent is that in systems where robust surfaces are used and nanobubbles are absent, consistent measurements of the true long range hydrophobic attraction are obtained, revealing an interaction that extends to surface separations of 10 - 20 nm[7, 10, 18-24]. The interaction can be fit with an exponential force profile where the pre-exponential term for very smooth surfaces is related to the energy of the hydrophobic surface in water and the decay length is up to 2 nm[21].

Given the high interfacial energy of hydrophobic surfaces is eliminated when they are brought into contact, it is unsurprising that such surfaces show strong adhesion and that a measurable hydrophobic attraction exists on approach, but the *range* of the attraction remains to be explained. For surfaces with contact angles greater than 90° the water film separating the surfaces is metastable, but at separations above 3 nm the energy barrier to cavitation ensures that the film remains metastable over relevant timescales[17]. The issue of the range of the hydrophobic attraction can be posed as simple question, how does a hydrophobic surface 'know' of another hydrophobic surface when they are separated by 10-20 nm? This infers that the perturbation from a single isolated extended hydrophobic surface extends at least half this distance. Electrostatic interactions can be ruled out as the force remains even in the presence of high concentrations of electrolyte[7]. If electrostatic interactions cannot explain the range of the hydrophobic attraction, perhaps perturbations of water structure can? Indeed perturbation of water structure was proposed as a mechanism for the hydrophobic

attraction as early as 1984[3], but a clear connection between water structure and the range of the attraction has not been established.

The structure of water adjacent to hydrophobic surfaces has been studied extensively, revealing that the loss of a hydrogen bond at the surface significantly alters the structure of the adjacent water leading to short range order[25]. X-ray and Neutron scattering studies, in line with other experiments and simulations[26-31], indicate that the perturbation of water structure adjacent to hydrophobic surfaces extends no further than the third hydration shell[32], which is incommensurate with an attraction that extends to separations of > 10 nm. However, these techniques are insensitive to long-range correlations in disordered media[33]. Whereas recently developed non-linear optical techniques that probe orientational fluctuations of molecules, that are sensitive to long-range order, report that the orientational order of water extends over distances of 5-15 nm using Hyper-Rayleigh Scattering (HRS)[34, 35] and Femtosecond Elastic Second Harmonic Scattering (fs-ESHS)[36]. The work of Shelton using HRS focuses on the solvent structure in the absence of electrolyte, whereas fs-ESHS senses the perturbation of orientational order of a solvent around an ion[33-35], finding that the correlations are long-ranged extending > 5 nm[36, 37]. It is notable in this work that the addition of a hydrophobic solute, CCl_4, showed no change in the fs-ESHS signal intensity. However, the ordering of water around a macroscopic hydrophobic surface is very different to the ordering around a hydrophobic solute[38-40]. In the latter no hydrogen bonds are lost and the density of water is enhanced around the solute, whereas in the former on average 1 hydrogen bond per water molecule is lost[39], so this does not exclude the orientational ordering adjacent to a hydrophobic solute from extending significant distances into solution.

It is known that the strength of the hydrophobic attractive force and adhesion is related to the hydrophobicity of the surfaces as measured by the contact angle[20]. Therefore, the accumulation of charge on a surface, which lowers the contact angle would be expected to reduce the hydrophobic attraction. However, the enhanced orientational order induced by ions suggests that in some circumstances surface charges may enhance the strength of the long-range hydrophobic attraction by strong perturbation of the water structure[34-36]. This effect may outweigh the small reduction in overall interfacial energy due to a small density of charge at the interface. It has already been shown that hydrophobic adhesive forces can be

amplified by the presence of a charge within 1 nm of a hydrophobic domain[41], but measurements on approach were not reported in this study, so it is unclear if the proximity of an ion can influence the range or the strength of the interaction out of contact. The above considerations lead to the hypothesis that the long-range nature of the hydrophobic attraction is a result of the long-range orientational correlation of water structure and this being the case the strength of the hydrophobic force between macroscopic surfaces may be enhanced in the presence of charges on the surface. In order to test this hypothesis we have measured the interaction forces between zinc sulfide (ZnS) surfaces. As ZnS surfaces are mildly hydrophobic there is no need to functionalize the surfaces, reducing the risk of producing forces that are associated with the reorganization of amphiphiles during the interaction of the surfaces[42, 43]. The charge on ZnS surfaces can readily be manipulated by changes in pH. Moreover, mildly hydrophobic surfaces are more likely to reveal the influence of charge on the hydrophobic attraction.

Materials and methods

All glassware used was cleaned by soaking in 10% NaOH solution for 10 minutes prior to rinsing with copious amount of pure water (Elga Chorus II, conductivity ~ 18.5 MΩ). The AFM fluid cell, O-ring, glass syringe, Teflon tubing and tweezers were rinsed with distilled ethanol and blown dry with clean nitrogen gas. Solutions of 1 mM sodium chloride were prepared using analytical grade NaCl (Sigma Aldrich) that had been roasted at 400^0C in an oven for 6 hours to remove any organic contaminants. The pH of the solution was adjusted using either HCl or NaOH solutions. Immediately prior to sputter coating, the substrates, cantilevers and colloid probes were cleaned with an RF water plasma system (40 W, 60 s, 125 kHz, ~ 0.1 torr) to remove any trace of organic contaminants.

Sample Preparation and Characterization

Magnetron sputtering was used to generate smooth ZnS surfaces suitable for direct force measurements. Prior to sputter coating, substrates and colloid probes were RF plasma cleaned at 40W for 60 seconds and used immediately. The vacuum chamber of a magnetron sputter coater (AJA, ATC2400) was filled with inert argon gas. The maximum sputtering power

was limited to 600 W with a starting pressure of 9 x 10^{-4} mTorr. In order to minimize contamination, pre-sputtering was performed for 10 minutes using 50% of maximum power on dummy silicon substrates. During sputtering an RF voltage was applied producing argon ions which impacted, in our case, a 3-inch diameter ZnS target (99.99% purity) resulting in ejection of ZnS from the target surface. This led to the coating of the samples placed in front of the target[44]. During deposition, the pressure was maintained at 4 mTorr and argon gas was maintained at a flow rate of 20 sccm during sputtering. The distance between the target and substrate was ~ 200 mm.

The thickness of the coating was determined using scanning angle spectroscopic ellipsometry (M200D, JA Woollam). By measuring the change in the polarization state of the reflected light off the substrate in question, it is possible to determine the optical properties and hence the film thickness on the substrate provided an appropriate optical model is used. The JA Woollam Co., Inc CompleteEASE™ analysis software was used to analyse the experimental data based on a silicon-ZnS layered optical model. The in-built silicon and ZnS optical models were obtained from Herzinger et. al[45] and Palik and Addamiano[46] respectively. In order to ascertain the quality of the thickness data, the Mean Squared Error (MSE) is evaluated. Multiple measurements on different ZnS substrates prepared on different occasions yielded MSE values of < 2 nm.

The substrates were imaged in ScanAsyst mode (Multimode VIII AFM, Bruker) using a ScanAyst Air cantilever, both before and after coating. The advancing and receding contact angle of water on the ZnS surfaces was measured using pH adjusted water via a KSV CAM200 contact angle goniometer which has a reported accuracy of ±1°. In order to create a droplet on the ZnS surface, a glass syringe attached to a blunt needle was used. Immediately after sputter coating, the ZnS surfaces were immersed in pH adjusted water for approximately 10 minutes before being blown dry with high purity nitrogen gas for the contact angle measurements. At each pH, the contact angle was measured at three or more different positions on three different substrates. The advancing (or receding) contact angles reported in this study are the maximum (or minimum) values immediately before the contact line moved upon addition (or removal) of solution.

X-ray Photoelectron Spectroscopy (XPS) was used to determine the chemical composition of the ZnS films, in particular the Zn:S ratio. The oxygen and carbon ratio was also measured to determine the degree of oxidation and adsorption of carbon contaminants from the atmosphere. The XPS was carried out using a Kratos Axis-Ultra spectrometer employing a monochromatic Al Kα X-ray source (1486.6 eV) operated at 130 W. Survey spectra were initially acquired with a pass energy of 160 eV, to quantify detected elements, in atomic %, using the appropriate elemental sensitivity factors. High-resolution spectra of the Zn 2p, S 2p, O 1s, and C 1s were acquired with a pass energy of 20 eV. Spectral fitting was accomplished CasaXPS (Casa Software). All samples were cooled, in vacuum, using a liquid-nitrogen-fed cold stage (temperature < −100 °C) to minimize photoreduction during exposure to X-rays during analysis[47].

Measurement and analysis of surface forces

Surface force measurements were repeated on four different occasions (using different surfaces and solutions) and were reproducible. Surface forces were measured by AFM (Nanoscope III, Digital instruments), equipped with a low noise head using the colloid probe technique[48, 49]. Prior to sputter coating, a borosilicate glass sphere of radius 10 ± 0.1 um (9020, Duke), was glued to the tip of a rectangular silicon nitride AFM cantilever (CSG 10,NT-MDT) using Epikote 1004 resin. The AFM cantilevers with attached colloid probes were examined and imaged after all experimental work was completed using a ZEISS Ultraplus Field Emission Scanning Electron Microscope (FESEM) to determine the radius of the particle. The spring constant of each cantilever was determined prior to colloid probe attachment via the inbuilt thermal tune[50] function of the Bruker ScanAsyst AFM, these varied between 0.1 N m^{-1} and 0.4 Nm^{-1}. Surface forces were measured in 1 mM NaCl at a range of pH between the spherical colloid probe and a boron doped silicon (100) wafer, (MEMC, U.S.A.) sputter coated with ZnS.

The analysis of the AFM data was performed using Derjaguin-Landau-Verwey-Overbeek (DLVO)[51, 52] theory extended to account for surface roughness (DLVO-R)[53]. This is a variant of the DLVO theory modified to account for surface roughness using a statistical description characterised by the RMS roughness, σ of each surface. In the DLVO-R theory, roughness

introduces two effects. Firstly, the short range noncontact forces of classical DLVO theory are magnified because of the reduced separation between outlying asperities. Secondly, elastic contact between asperity tips introduces a repulsive force, which in some instances may mask attractive Van der Waals forces between surfaces[54, 55]. The contact force is determined by the elastic Young's modulus of the surface materials and the average curvature of asperity tips, in conjunction with RMS roughness. In the application of conventional DLVO theory, the surface potential is fitted until the theoretical curve best matches a measured force curve. In DLVO-R applications, the surface potential and asperity tip radius are fitted, with RMS roughness estimated from reflectometry/AFM measurements or from a histogram of surface heights measured by AFM. See section S5 of the SI for further details.

Results and Discussion

A number of previous studies have investigated the interaction forces using ZnS surfaces[56-60]. Researchers have recognized that a particular challenge has been preparing surfaces that are very smooth. In one study the RMS roughness of the ZnS sphere was reported to be 3.5 nm RMS over a small area[59]. This complicates the interpretation of the forces measured as even small levels of roughness can be sufficient to obscure short range attractive forces[53, 55, 61]. The nature of the forces will not only depend on the pH of solution but also the other ions in solution[58] and considering the roughness of the surfaces used in earlier studies our results in general cannot be directly compared to previous studies which also employed different solution conditions, motivated by understanding the flotation behavior of ZnS[57-59].

Characterization of ZnS surfaces

A range of sputtering power and deposition times were employed to produce ZnS films. We found that a lower sputtering power led to a smoother ZnS surface, due to a reduction in grain size. Elevated temperatures were not employed as this has been shown to result in an increase in grain size, and an increase in surface roughness[62, 63]. An AFM image and line profile from the image of a ZnS sputter coated film (10 mins, 150 W) is presented in Fig. 1. Analysis of the image gives an RMS surface roughness of 0.68 nm, which is a moderate increase on the RMS roughness of the uncoated surface (0.22 nm). The thickness of the ZnS layer was determined by ellipsometry to be 34.5 ± 1.3 nm with a refractive index of 2.28 at a wavelength

of 600 nm. This is in accordance with the refractive index reported in the literature[64]. The stated error is the root mean square error in coating thickness across different samples.

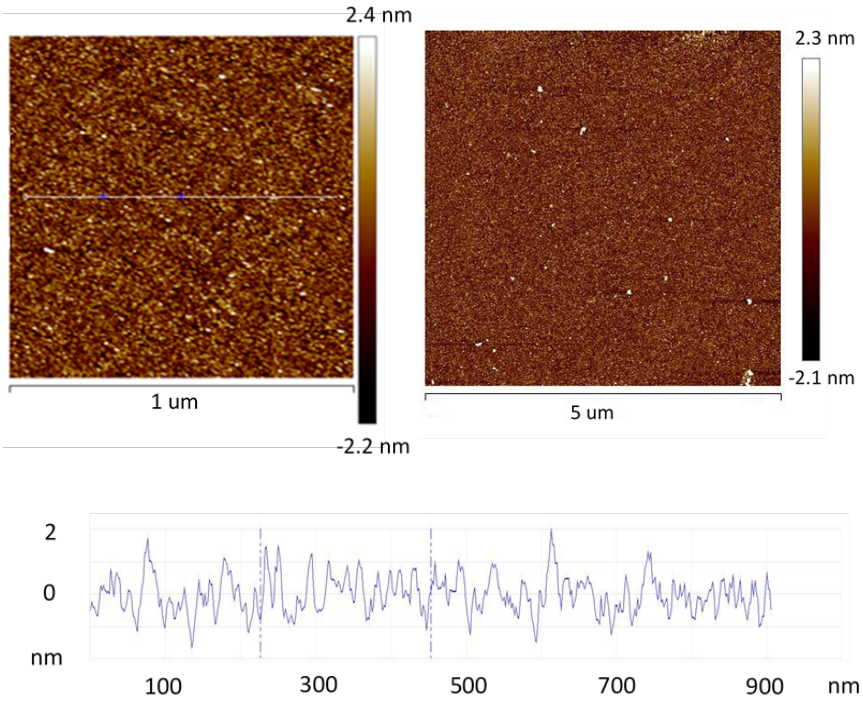

Figure 1 Atomic Force Microscope (1 um x 1 um) image of a ZnS coated silicon wafer (Top left) obtained in ScanAsyst mode. Analysis of the images reveals an RMS surface roughness of 0.68 nm. The same surface imaged over a larger scan size (5 um x 5 um) gave an RMS surfaces roughness of 0.71 nm (Top Right). The profile of a section from the top left image marked by a white line is shown in the bottom panel. The coating was produced by magnetron sputtering for 10 minutes at 150W.

Colloid probes were sputter coated with ZnS at the same time (and therefore under the same conditions) as flat substrates. Hence, the thickness on the colloid probe is assumed to be the same as on the flat substrate. The surface of the coated colloid probe was imaged using the AFM reverse imaging technique[65] and is shown in Fig. 2 for a scan size of 500 nm x 500 nm. From this image, the surface roughness of the region of the colloid probe that came into contact with the substrate during the AFM force measurements was measured to have an RMS roughness of 0.51 nm.

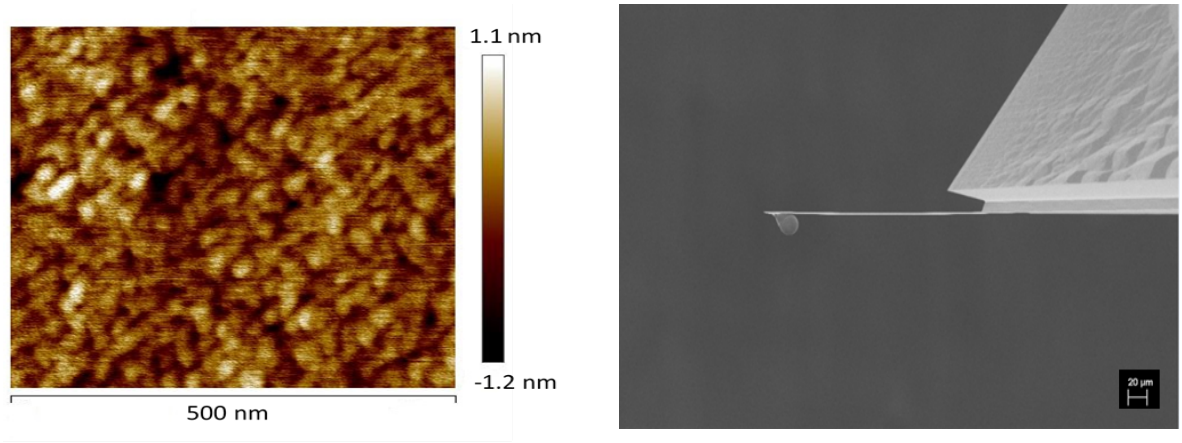

Figure 2 AFM image of a colloid probe acquired using the reverse imaging technique (left panel)[65]. This involves using the colloid probe to image a calibration grating (TGT01 Micromasch) which consists of an array of sharp spikes. This results in an image of the region of the colloid probe that interacts during force measurements being obtained for each spike. Analysis of the image of the ZnS-coated colloid probe showed an RMS roughness of 0.51 nm over an area of 500 nm x 500 nm. A FESEM image of an AFM cantilever with a ZnS coated sphere attached to the tip taken after measurement is shown in the right panel.

The compositions of the ZnS films were measured using X-Ray photoelectron sputtering (XPS), see supporting Information Fig. S1. This revealed that the sputter coated ZnS surface has a Zn:S ratio of 1.24 : 1, whereas the stoichiometric ratio is 1:1, see supporting Information Table S1. Oxidation and adventitious hydrocarbon contamination accounts for the discrepancy and some sulphur atoms have been replaced with oxygen atoms or hydroxyl groups. A similar Zn:S ratio of 1.23 was reported for ZnS deposited using a chemical bath[66]. The effect of deposition temperature on the structure of ZnS deposited via RF magnetron sputtering has been studied by Hwang et al[62]. In this study, the samples were also non-stoichiometric although the stoichiometry improved at higher deposition temperatures such that at 350°C, the Zn:S ratio approaches 1. The high resolution spectra for the Zn 2p and S 2p, were consistent with ZnS in either the zincblende (sphalerite) or wurzite structure, with the Zn 2p3/2 and S 2p3/2 located at 1021.9 eV and 162.8 eV binding energy respectively[67]. The X-ray excited valence band spectrum of the ZnS film was consistent with bulk ZnS in the zincblende (sphalerite) form as reported by Ley et al.[68].

Wettability of ZnS surfaces

To characterise the wettability of the sputtered ZnS surfaces the advancing and receding contact angles of water were measured on freshly coated ZnS surfaces as a function of pH.

The advancing contact angles, shown in Fig. 3, exhibit a weak, or negligible, dependence on pH and were found to lie between 43° and 33°. These measurements indicate that these surfaces are less hydrophobic than surfaces that typically give rise to hydrophobic forces. The long range hydrophobic attraction has often been reported between surfaces with advancing contact angles less than 90°, such as silica surfaces with physisorbed surfactant films, where the advancing contact angle may be as low as 65°[1]. Recent experiments show that a substantial hydrophobic attraction is evident when one surface has a contact angle of only 40°[20]. The low contact angles measured on the ZnS surfaces used in this study makes an attraction due to cavitation between the surfaces unlikely. As shown in Fig. 3, there is a hysteresis between the advancing and receding contact angles.

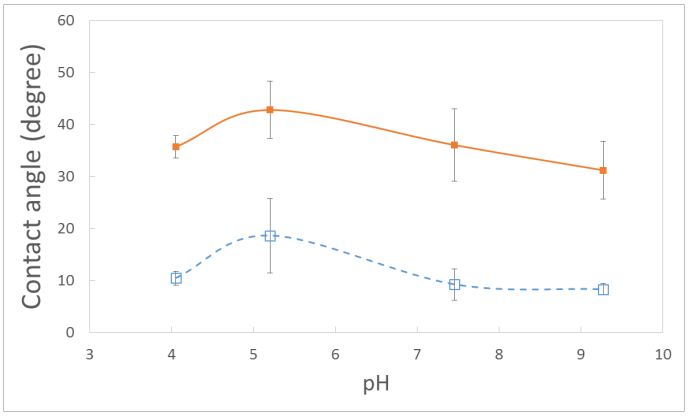

Figure 3 Advancing (solid symbols) and receding (open symbols) contact angles of water on freshly prepared ZnS surfaces as a function of pH. The error bars denote the standard deviation for the values measured over at least 3 repetitions at different locations on at least 3 different substrates. Lines are to guide the eye.

Van der Waals Force Theory for Layered Systems

The van der Waals interaction between surfaces is commonly represented by a single Hamaker constant. The Hamaker constant for the bulk ZnS-water-ZnS interaction[69, 70] has a value of 6.09×10^{-20} J for hexagonal ZnS (wurtzite), and 5.31×10^{-20} J for cubic ZnS (sphalerite). However, in our system ZnS forms a thin layer on a silica sphere or flat silica/silicon substrate. Evaluation of the van der Waals interaction of a multilayer system is similar to that for a bulk 3-phase interaction[71]. The chief quantity used to compute van der Waals energies is the dielectric reflection coefficient Δ at the interface between each layer, which describes the difference in the response of the two materials on either side of an interface to an electric field. The retarded reflection coefficient is $\Delta_{ij}=(\varepsilon_i-\varepsilon_j)/(\varepsilon_i+\varepsilon_j)$ where ε_i and ε_j are the dielectric

functions of each material, hexagonal ZnS[69] , water[70 72], Si and SiO_2[73], taken predominantly over imaginary optical/UV frequencies (the full calculation includes retardation due to the finite speed of light). In a multi-layered system the reflection coefficients are evaluated recursively[71], taking each interface in turn, weighted by the thickness of each layer[54]. At close range (< 10 nm) the overall interaction follows that of bulk ZnS-water-ZnS. At longer separations the effective Hamaker coefficient falls steadily from the pure ZnS value of 6.09×10^{-20} J, reaching the smaller value of 1.63×10^{-20} J, due to the underlying silica substrates at a separation of 200 nm. The calculated distance dependent Hamaker coefficient as a function of separation is presented in Fig. S2 of the supporting information.

Surface force measurements

The interaction forces between ZnS surfaces were measured as a function of pH. Firstly we discuss the interaction force at the isoelectric point (iep) of the ZnS surface, as shown in Fig. 4. At this pH of 7.1, there is no evidence of a repulsive force between the ZnS-coated colloid probe and substrate at any separation, indicating the lack of any significant electrostatic repulsion. This indicates that the surface potential must be close to zero, indicating the isoelectric point (iep) occurs at pH 7.1. A monotonic attraction is evident from a separation of ~ 35 nm. The attractive interaction is described well by the Lifshitz calculation of the Van der Waals interaction. (see Fig. 4). The surfaces jump to contact from a separation of ~ 9 nm as the gradient of the attractive force exceeds the spring constant of the cantilever causing a mechanical instability. This result confirms previous assessments that aggregation of ZnS particles at pH ~ 7 is not due to hydrophobic forces but can be explained by van der Waals attraction at the iep[58].

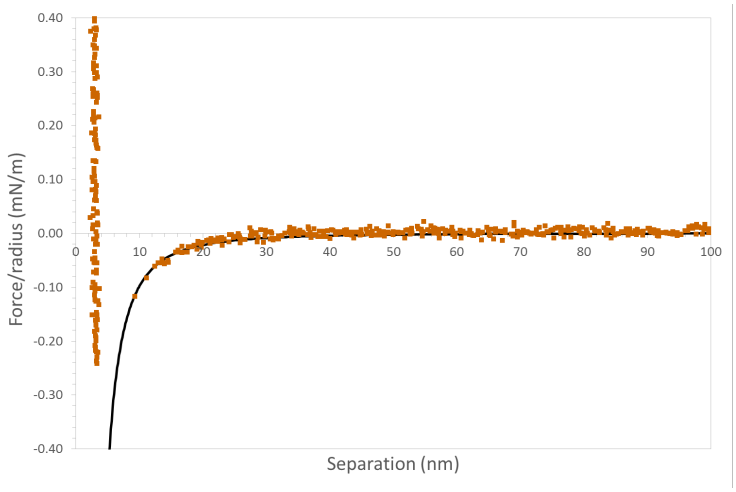

Figure 4 Normalized approach force between ZnS surfaces at pH 7.1 in 10^{-3} M NaCl. The calculated Van der Waals interaction is shown as a solid line for comparison (see text for details). The force curve measured at pH 7.1 fits the calculated van der Waals interaction without any fitting parameters indicating that the system is at the iep. The steeply repulsive interaction is due to asperity contact and is therefore offset from the zero of separation which corresponds to the average height of the mildly rough interfaces.

Increasing the pH above the iep will cause the surfaces to acquire a negative charge. The interaction measured on approach at pH 9.8 in 1 mM NaCl shows a repulsion at separations > 10 nm and an attraction at separations < 10 nm which results in the surfaces jumping into contact, see Fig. 5. Theoretically, the electrostatic interaction is bounded by two limits, the surface charge may remain constant during the interaction (upper solid line), or the charge can regulate such that the surfaces maintain a constant potential (lower dashed line). Real surfaces will generally charge regulate between these limits. The fitting curve was obtained with a surface potential -21 mV, an a Debye length of 9.7 nm. Note there is no direct evidence of the long-range hydrophobic attraction at this pH, as the jump to contact (shown by the red arrow) is consistent with DLVO theory for surfaces that charge regulate under a constant potential boundary condition. An alternative explanation is that the charge regulation is hindered and the situation is closer to the constant charge boundary condition and the jump to contact is indicative of a small hydrophobic attraction.

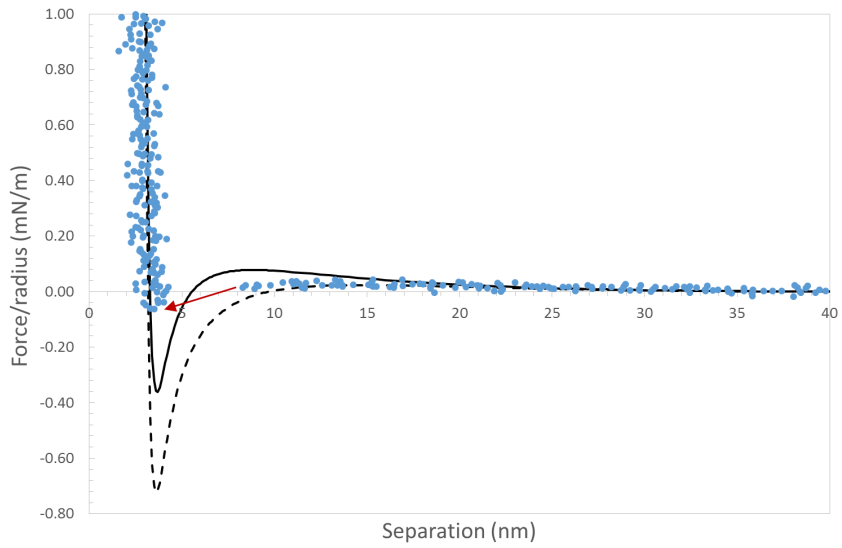

Figure 5 The normalized approach force at pH 9.8 in 10^{-3}M NaCl. The data is fit using the DLVO theory accounting for surface roughness (DLVO-R) using a surface roughness of RMS 0.68 nm for the substrate and RMS 0.51 nm for the colloid probe, ψ = -21 mV and κ^{-1} = 9.7 nm which is corresponds to a 1:1 electrolyte concentration of 0.98 x 10^{-3} M). The dispersion forces were calculated using Lifshitz theory as described above. The two lines show the different boundary conditions of constant charge (solid) and constant potential (dashed). The arrow indicates the instance when the two surfaces jump into contact due to the instability of the cantilever. The steeply repulsive

interaction is due to asperity contact and is therefore offset from the zero of separation which corresponds to the average height of the mildly rough interfaces.

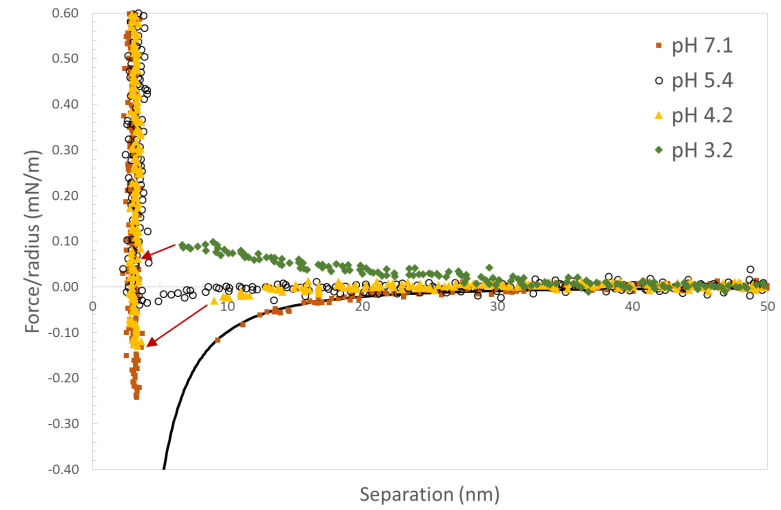

Figure 6 Normalized approach force between ZnS surfaces in 10^{-3}M NaCl on a linear scale between pH 7.1 and pH 3.2. Forces generated using RMS 0.68 nm for the substrate and RMS 0.51 nm for the colloid probe. At pH 5.4 the electrostatic repulsion increases, reducing the magnitude of the attraction at small separations. At pH 3.2 the electrostatic repulsion is more evident. The interaction at pH 4.2 is inconsistent with DLVO theory in that the attraction is greater than observed for pH 5.4, when the electrostatic repulsion will have increased. Arrows indicate when the surfaces jump into contact due to the instability of the cantilever. The steeply repulsive interaction is due to asperity contact and is therefore offset from the zero of separation which corresponds to the average height of the mildly rough interfaces.

Below the iep we expect that the surfaces will acquire a positive charge that increases with decreasing pH. The interaction forces measured on approach at pH 7.1, pH 5.4, pH 4.2 and pH 3.2 are shown in Fig. 6. At pH 5.4, the interaction is less attractive than at pH 7.1, indicating that the surfaces have acquired a small positive surface charge leading to a small electrostatic repulsion that decreases the overall attraction. It is not possible to accurately determine the surface potential from a DLVO-R fit to the data because for small magnitudes of the surface potential the difference in the constant charge and constant potential boundary conditions are large, thus the error in the fitted potential is large. At pH 3.2 the repulsion is more substantial indicating that the surfaces have acquired a greater positive charge and the electrostatic repulsion has consequently increased. This is consistent with measurements of the zeta potential of ZnS particles[74, 75]. The interaction at pH 3.2 is fit using DLVO-R theory in Fig. 7 with a surface potential of +24 mV and Debye length of 9.2 nm in line with expectations.

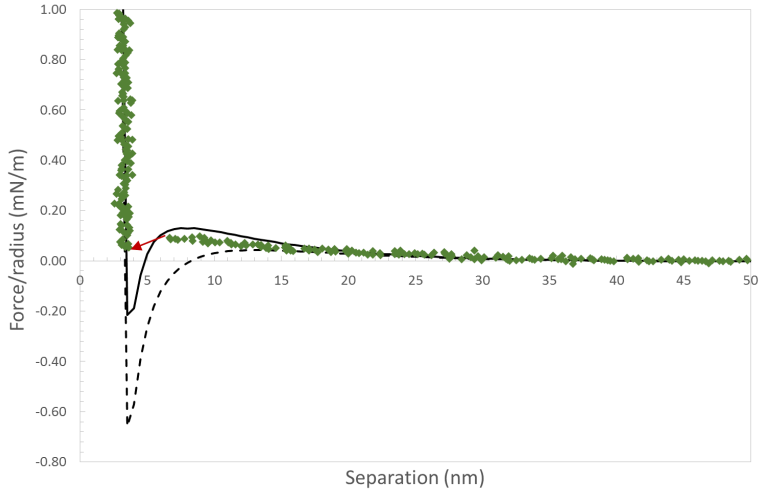

Figure 7 Normalized approach force at pH 3.2 in 10^{-3}M NaCl on a linear scale. (DLVO-R fit shown using surface roughness of RMS 0.68 nm for the substrate and RMS 0.51 nm for the colloid probe, ψ = +24 mV and κ^{-1} = 9.2 nm which is consistent with a 1:1 electrolyte concentration of 1.1 x 10^{-3} M). The arrow indicates the instance when the two surfaces jump into contact due to the instability of the cantilever. The two lines show the different boundary conditions of constant charge (solid) and constant potential (dashed).

The data measured at pH 4.2 cannot be explained by DLVO theory as the interaction is more attractive than the interaction measured at pH 5.4 despite the pH being further from the iep, which should result in a greater repulsion due to an increase in positive surface charge as expected from zeta potential measurements on ZnS surfaces with the same iep, which show a an increase in zeta potential over this range of pH [74, 75].We attribute the extra attraction to the long range hydrophobic attraction and note that a previous study reported an anomalous attraction of similar range between ZnS surfaces at pH 4.0 and attributed it to the hydrophobic attraction[59]. These observations are also consistent with measurements of the yield stress that show two maximums, one at the iep (pH~ 7) and the other at pH < 4[74]. In this work, the hydrophobic attraction was a maximum at pH 4.2 but reduced only slightly when the pH was increased to pH 4.8 or reduced to pH 3.8, see supporting Information figure S3. In this pH range the surfaces have acquired a small positive charge. Thus the measurable hydrophobic attraction is evident over a pH range of 1 unit. At the iep (pH 7.1) where there is no net positive charge the interaction was fully described by the calculated van der Waals interaction. This strongly suggests that the hydrophobic attraction is amplified by the presence of positive charges on the surface. If this is indeed the case we would expect a commensurate increase in adhesion when the hydrophobic attraction is acting.

Adhesion Measurements

Surfaces that interact strongly with water exhibit an additional non-DLVO hydration repulsion associated with the need to remove water that is solvating surface groups when surfaces are brought close to contact[76-78]. The hydration force is not present between more hydrophobic surfaces that do not interact strongly with water. The presence of a hydration force often prevents adhesion between hydrophilic surfaces such as silica[48, 77] which DLVO theory (which does not include hydration forces) predicts would show a strong adhesion. As such adhesion forces are useful for investigating the hydrophobicity of a surface[41]. To explore this, the forces between ZnS surfaces were also measured during separation (See supporting Information Fig. S4 for examples of individual measurements). The interaction is found to be hysteretic between approach and separation at all pH values and adhesion is seen in all cases, indicating the hydrophobic nature of the surfaces across the full range of pH investigated. For example, at pH 9.8, although there was a small repulsive electrostatic force during approach, the surfaces adhered when in contact. This also indicates that adhesion measurements are more sensitive to hydrophobicity than measurements of the surface forces on approach, though they are inherently more variable. The variability is a result of the small contact area, surface roughness and possibly also twisting or peeling motions associated with bending of the cantilever.

Frequency histograms of the adhesion forces measured as a function of pH are presented in Fig. 8 and the maximum, mean and median adhesion measured at different pH is summarised in Table S2 in the supporting information. For a given pH, repeated measurements at the same location showed no difference to those measured at different locations. It is notable that the largest adhesion was not measured at the iep (pH 7.1) but at pH 4.2 where the extra attraction was observed in the approach curve. Much smaller adhesions were measured at pH 9.8, pH 5.4 and pH 3.2. The histogram at pH 3.2 and 5.4 is bimodal suggesting two different classes of adhesion events, the larger of which overlap with the adhesion forces measured at pH 4.2. This suggests that the smaller adhesion events are due to van der Waals interactions and the larger adhesion events are due to hydrophobic attraction, enhanced by the presence of cations on the surface (H+ ions forming part of the $-ZnOH_2^+$ surface group) . It is not possible here to compare these measurements with predictions from JKR theory due to the influence

of surface roughness. These measurements are consistent with the reports of an increase in hydrophobic adhesion associated with the proximal location of a cationic charge near a hydrophobic moiety using an AFM tip [41].

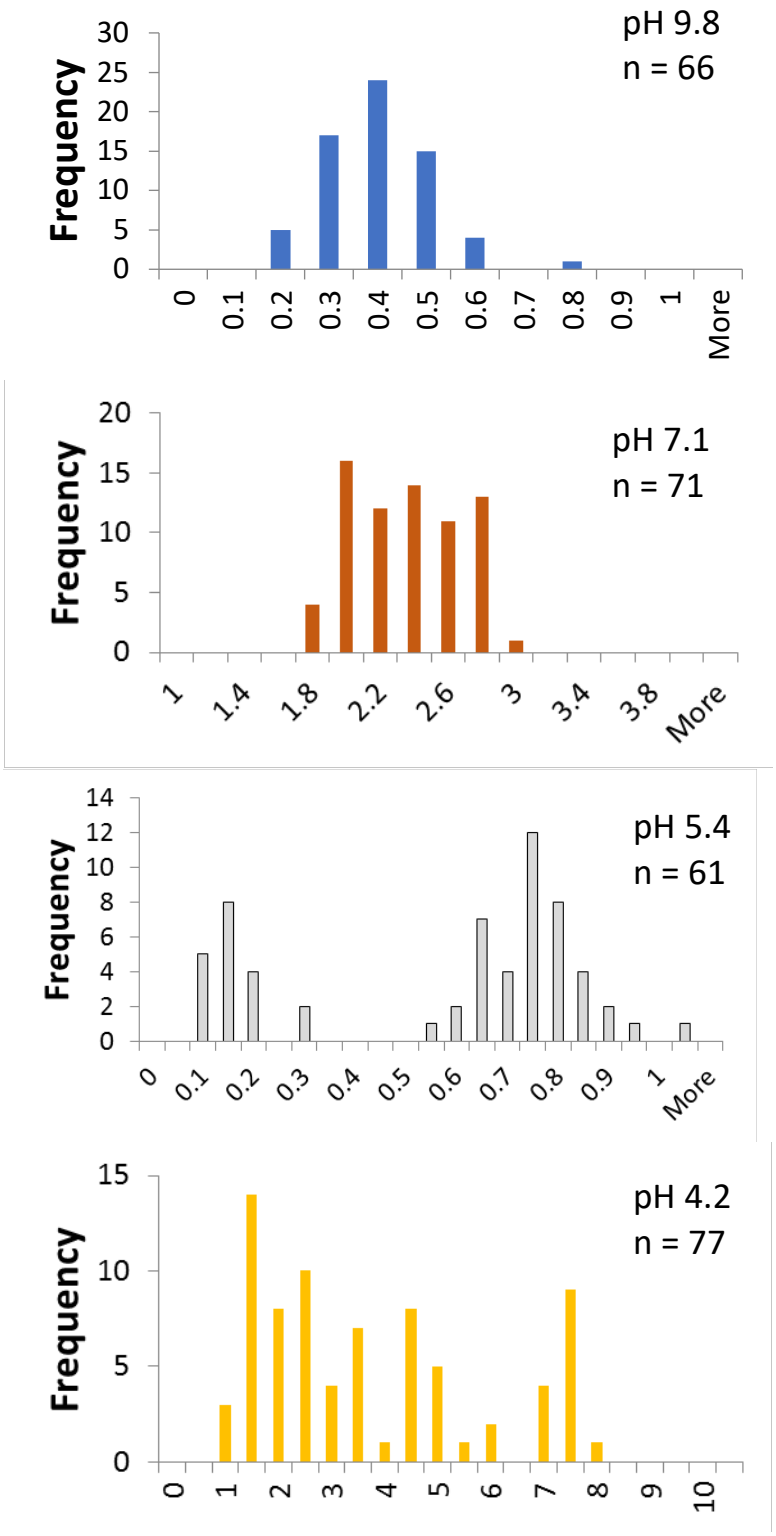

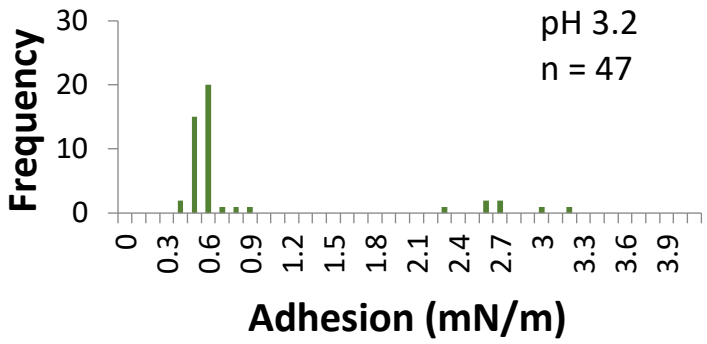

Figure 8 Frequency histograms of the normalised adhesion forces between ZnS surfaces at a range of pH values. The y-axis represents the frequency of the measured interactions with a particular range of normalised adhesion forces. Note the range of the x axis and the bin size (n) vary.

The measurements reported here are consistent with the long-range hydrophobic attraction being mediated by long-range correlations in the orientation of water molecules which are reported to have a similar range. These correlations are reported by Shelton[34] to be present in bulk water at distances comparable to the range of the hydrophobic attraction and are reported by Chen et al.[36] to be enhanced by ions in solution over the appropriate range for the hydrophobic attraction. The suggestion being that the structure of water is perturbed at extended hydrophobic interfaces and that this perturbation is communicated across distances of 5 -10 nm from each surface through changes in the orientational order of water molecules. As the surfaces approach, this ordered water is released leading to an attraction. The range of the hydrophobic attraction between liquid surfaces is notably less than for solid surfaces[79]. This may arise as the fluid nature of the liquid interface, which will be in motion due to capillary waves, is less able to order the structure of water. Additionally, recent work investigating the influence of the molecular order in hydrophobic self-assembled monolayers has observed an increase in the strength of hydrophobic adhesion for surfaces that a more ordered[80], consistent with the possibility that the strength of the hydrophobic attraction is dependent upon and transmitted by the perturbation of water structure at a hydrophobic surface. In this study for both the forces measured on approach and separation the presence of cations is seen to increase the hydrophobic interaction, suggesting that the presence of cations enhances the orientational ordering of water as seen in fs-ESHS[36]. This is consistent with earlier work where the hydrophobic adhesion was amplified in the presence of cations[41]. At an extended hydrophobic interface hydrogen bonding is reduced and the density of water is reduced leading to greater fluctuations in water density at the interface[39]. The presence of

a small number of ions which locally attract water will reduce density fluctuations and in this way may thereby enhance the ability of the surface to order water, whilst only having a minor effect on the overall interfacial energy (ie hydrophobicity). This work also suggests a connection between the hydrophobic effect and the long range hydrophobic interaction in that they are both mediated by water structure. However it remains to be seen how the range of the interaction scales with the size of the hydrophobic region and precisely how the local topography influences these interactions.

Conclusions

The interaction forces have been measured between zinc sulphide surfaces as a function of pH. The iep is at pH 7.1 as indicated by an attractive interaction that is well described by the Van der Waals attraction calculated using Lifshitz theory. At higher pH values the surfaces show a DLVO interaction due to a negative surface potential. At lower pH values the surfaces show a DLVO interaction due to a positive surface potential. Forces measured in the pH range of 3.8 to 4.8 showed an additional attractive component that is attributed to the long-range hydrophobic attraction. Upon separating the surfaces adhesive forces were measured over the full range of pH, but were significantly larger at pH 4.2, due to hydrophobic interactions. The range of the hydrophobic forces is consistent with the range of orientational correlations of water revealed by harmonic spectroscopic methods. The enhanced hydrophobic interactions observed here on approach and separation of the surfaces when the surface is positively charged is consistent with previous reports that observed increased hydrophobic adhesion due to cations located in proximity to hydrophobic sites and suggests that the presence of positive charges on the hydrophobic surface may increase the strength of orientational correlations that communicate the hydrophobic force through perturbation of water structure.

Acknowledgements

This magnetron sputtering was performed in the ACT node of the Australian National Fabrication Facility, a facility established under the National Collaborative Research Infrastructure Strategy to provide nano and micro-fabrication facilities for Australian based researchers. The Centre of Advanced Microscope (CAM) at ANU provided FESEM access and expertise. V.S.J. Craig gratefully acknowledges support from the Australian Research Council through a Discovery Grant, DP140102371.

Supporting information: The following supporting information is available for download: XPS spectra of the Zinc Sulphide surfaces used in this study; Calculated distance dependent Hamaker Coefficients for ZnS coated surfaces; Effect of pH on the measured force in the range 3.8 < pH < 4.8 and Effect of pH on the measured adhesion between ZnS surfaces; Fitting of force measurement data using DLVO-R.

References

1. J. Israelachvili and R. Pashley, *Nature*, 1982, **300**, 341-342.
2. W. A. Ducker and D. Mastropietro, *Curr Opin Colloid In*, 2016, **22**, 51-58.
3. J. N. Israelachvili and R. M. Pashley, *J. Colloid Interface Sci.*, 1984, **98**, 500-514.
4. R. Pashley, P. McGuiggan, B. Ninham and D. Evans, *Science*, 1985, **229**, 1088-1089.
5. P. M. Claesson, C. E. Blom, P. C. Herder and B. W. Ninham, *J. Colloid Interface Sci.*, 1986, **114**, 234-242.
6. K. Kurihara and T. Kunitake, *J. Am. Chem. Soc.*, 1992, **114**, 10927-10933.
7. L. Meagher and V. S. J. Craig, *Langmuir*, 1994, **10**, 2736-2742.
8. J. L. Parker and P. M. Claesson, *Langmuir*, 1994, **10**, 635-639.
9. V. S. J. Craig, B. W. Ninham and R. M. Pashley, *Langmuir*, 1998, **14**, 3326-3332.
10. N. Ishida, M. Sakamoto, M. Miyahara and K. Higashitani, *Langmuir*, 2000, **16**, 5681-5687.
11. N. Ishida and K. Higashitani, *Miner. Eng.*, 2006, **19**, 719-725.
12. R. F. Tabor, D. Y. C. Chan, F. Grieser and R. R. Dagastine, *J. Phys. Chem. Lett.*, 2011, **2**, 434-437.
13. V. S. J. Craig, *Soft Matter*, 2011, **7**, 40-48.
14. J. L. Parker, P. M. Claesson and P. Attard, *J. Phys. Chem.*, 1994, **98**, 8468-8480.

15. S. T. Lou, Z. Q. Ouyang, Y. Zhang, X. J. Li, J. Hu, M. Q. Li and F. J. Yang, *J. Vac. Sci. Technol., B:*, 2000, **18**, 2573-2575.
16. N. Ishida, T. Inoue, M. Miyahara and K. Higashitani, *Langmuir*, 2000, **16**, 6377-6380.
17. K. Leung, A. Luzar and D. Bratko, *Phys. Rev. Lett.*, 2003, **90**.
18. N. Ishida, Y. Kusaka and H. Ushijima, *Langmuir*, 2012, **28**, 13952-13959.
19. N. Ishida, Y. Kusaka and H. Ushijima, *Chem. Lett.*, 2012, **41**, 1273-1275.
20. N. Ishida, K. Matsuo, K. Imamura and V. S. J. Craig, *Langmuir*, 2018, **34**, 3588-3596.
21. S. H. Donaldson, A. Royne, K. Kristiansen, M. V. Rapp, S. Das, M. A. Gebbie, D. W. Lee, P. Stock, M. Valtiner and J. Israelachvili, *Langmuir*, 2015, **31**, 2051-2064.
22. E. E. Meyer, K. J. Rosenberg and J. Israelachvili, *Proc. Nat. Acad. Sci.*, 2006, **103**, 15739-15746.
23. M. Hato, *The Journal of Physical Chemistry*, 1996, **100**, 18530-18538.
24. G. E. Yakubov, H.-J. Butt and O. I. Vinogradova, *J. Phys. Chem. B*, 2000, **104**, 3407-3410.
25. C. Holzl and D. Horinek, *Phys. Chem. Chem. Phys.*, 2018, **20**, 21257-21261.
26. R. Buchner, G. T. Hefter and P. M. May, *J. Phys. Chem. A*, 1999, **103**, 1-9.
27. S. Bouazizi, S. Nasr, N. Jaidane and M. C. Bellissent-Funel, *J. Phys. Chem. B*, 2006, **110**, 23515-23523.
28. Y. Marcus and G. T. Hefter, *Chem. Rev.*, 2006, **106**, 4585-4621.
29. R. Mancinelli, A. Botti, F. Bruni, M. A. Ricci and A. K. Soper, *Phys. Chem. Chem. Phys.*, 2007, **9**, 2959-2967.
30. A. Nilsson, D. Nordlund, I. Waluyo, N. Huang, H. Ogasawara, S. Kaya, U. Bergmann, L. A. Naslund, H. Ostrom, P. Wernet, K. J. Andersson, T. Schiros and L. G. M. Pettersson, *J. Electron Spectrosc.*, 2010, **177**, 99-129.
31. S. Funkner, G. Niehues, D. A. Schmidt, M. Heyden, G. Schwaab, K. M. Callahan, D. J. Tobias and M. Havenith, *J. Am. Chem. Soc.*, 2012, **134**, 1030-1035.
32. M. C. Bellissent-Funel, R. Sridi-Dorbez and L. Bosio, *J. Chem. Phys.*, 1996, **104**, 10023-10029.
33. D. P. Shelton, *J. Chem. Phys.*, 2012, **136**, 044503.
34. D. P. Shelton, *J. Chem. Phys.*, 2014, **141**, 224506.
35. D. P. Shelton, *J. Chem. Phys.*, 2017, **147**, 214505.
36. Y. Chen, H. I. Okur, N. Gomopoulos, C. Macias-Romero, P. S. Cremer, P. B. Petersen, G. Tocci, D. M. Wilkins, C. Liang, M. Ceriotti and S. Roke, *Science Advances*, 2016, **2**.
37. Y. Chen, N. Dupertuis, H. I. Okur and S. Roke, *J. Chem. Phys.*, 2018, **148**, 222835.
38. K. Lum, D. Chandler and J. D. Weeks, 1999, **103**, 4570-4577.
39. D. Chandler, *Nature*, 2005, **437**, 640-647.
40. D. Ben-Amotz, in *Annual Review of Physical Chemistry, Vol 67*, eds. M. A. Johnson and T. J. Martinez, Annual Reviews, Palo Alto, 2016, vol. 67, pp. 617-+.
41. C. D. Ma, C. Wang, C. Acevedo-Velez, S. H. Gellman and N. L. Abbott, *Nature*, 2015, **517**, 347-350.
42. E. E. Meyer, Q. Lin, T. Hassenkam, E. Oroudjev and J. N. Israelachvili, *Proc. Nat. Acad. Sci.* , 2005, **102**, 6839-6842.
43. S. Perkin, N. Kampf and J. Klein, *J. Phys. Chem. B*, 2005, **109**, 3832-3837.
44. P. J. Kelly and R. D. Arnell, *Vacuum*, 2000, **56**, 159-172.
45. C. M. Herzinger, B. Johs, W. A. McGahan, J. A. Woollam and W. Paulson, *J. Appl. Phys.*, 1998, **83**, 3323-3336.

46. E. D. Palik and A. Addamiano, in *Handbook of Optical Constants of Solids*, Academic Press, Burlington, 1997, DOI: https://doi.org/10.1016/B978-012544415-6.50030-3, pp. 597-619.
47. W. M. Skinner, C. A. Prestidge and R. S. C. Smart, *Surf. Interface Anal.*, 1996, **24**, 620-626.
48. W. A. Ducker, T. J. Senden and R. M. Pashley, *Nature*, 1991, **353**, 239-241.
49. H.-J. Butt, *Biophysical Journal*, 1991, **60**, 1438-1444.
50. J. L. Hutter and J. Bechhoefer, *Rev. Sci. Instrum.*, 1993, **64**, 1868-1873.
51. B. V. Derjaguin and L. Landau, *Acta. Physicochem. URSS*, 1941, **14**, 633.
52. E. J. W. Verwey and J. T. G. Overbeek, *Theory of the Stability of Lyophobic Colloids*, Elsevier, Amsterdam, The Netherlands, 1948.
53. D. F. Parsons, R. B. Walsh and V. S. J. Craig, *J. Chem. Phys.*, 2014, **140**, 164701.
54. R. Walsh, A. Nelson, W. M. Skinner, D. Parsons and V. S. J. Craig, *J. Phys. Chem. C*, 2012, **116**, 7838-7847.
55. N. Eom, D. F. Parsons and V. S. J. Craig, *J. Phys. Chem. B*, 2017, **121**, 6442-6453.
56. D. T. Atkins and R. M. Pashley, *Langmuir*, 1993, **9**, 2232-2236.
57. T. H. Muster, G. Toikka, R. A. Hayes, C. A. Prestidge and J. Ralston, *Colloids Surf. A.*, 1996, **106**, 203-211.
58. G. Gillies, M. Kappl and H. J. Butt, *Langmuir*, 2005, **21**, 5882-5886.
59. G. Toikka, R. A. Hayes and J. Ralston, *Langmuir*, 1996, **12**, 3783-3788.
60. Z. Xu, R. Chi, T. Difeo and J. A. Finch, *J. Adhes. Sci.Technol.*, 2000, **14**, 1813-1827.
61. E. Thormann, *Curr Opin Colloid In*, 2017, **27**, 18-24.
62. D. H. Hwang, J. H. Ahn, K. N. Hui, K. S. Hui and Y. G. Son, *Nanoscale Res. Lett.*, 2012, **7**, 26-26.
63. S. P. Patel, J. Pivin, V. S. Kumar, A. Tripathi, D. Kanjilal and L. Kumar, *Vacuum*, 2010, **85**, 307-311.
64. H. Li, *J. Phys. Chem. Ref. Data*, 1984, **13**.
65. C. Neto and V. S. J. Craig, *Langmuir*, 2001, **17**, 2097-2099.
66. T. Ben Nasr, N. Kamoun and C. Guasch, *Appl. Surf. Sci.*, 2008, **254**, 5039-5043.
67. C. A. Prestidge, W. M. Skinner, J. Ralston and R. S. C. Smart, *Appl. Surf. Sci.*, 1997, **108**, 333-344.
68. L. Ley, R. Pollak, F. McFeely, S. P. Kowalczyk and D. Shirley, *Phys. Rev. B*, 1974, **9**, 600.
69. L. Bergstrom, *Adv. Colloid Interface Sci.*, 1997, **70**, 125-169.
70. R. R. Dagastine, D. C. Prieve and L. R. White, *J. Colloid Interface Sci.*, 2000, **231**, 351-358.
71. V. A. Parsegian and B. W. Ninham, *J. Theor. Biol.*, 1973, **38**, 101-109.
72. T. J. Senden and C. J. Drummond, *Coll. Surf. A-Physicochem. Eng. Asp.*, 1995, **94**, 29-51.
73. A. Grabbe, *Langmuir*, 1993, **9**, 797-801.
74. T. H. Muster and C. A. Prestidge, *Miner. Eng.*, 1995, **8**, 1541-1555.
75. J. C. Liu and C. P. Huang, *Langmuir*, 1992, **8**, 1851-1856.
76. V. A. Parsegian and T. Zemb, *Curr Opin Colloid In*, 2011, **16**, 618-624.
77. A. Grabbe and R. G. Horn, *J. Colloid Interface Sci.*, 1993, **157**, 375-383.
78. V. A. Parsegian, R. P. Rand and N. L. Fuller, *J. Phys. Chem.*, 1991, **95**, 4777-4782.
79. R. F. Tabor, C. Wu, F. Grieser, R. R. Dagastine and D. Y. C. Chan, *J. Phys. Chem. Lett.*, 2013, **4**, 3872-3877.
80. H. Yeon, C. X. Wang, R. C. Van Lehn and N. L. Abbott, *Langmuir*, 2017, **33**, 4628-4637.

TOC figure

Surface force measurements reveal that a small increase in surface charge enhance the long range hydrophobic attraction.